Detection of tumour in biological tissues by laser backscattering and transillumination signal analysis

J. B. Jeeva[1] and Megha Singh[1,2,*]

[1]Division of Biomedical Engineering, School of Biosciences and Technology, VIT University, Vellore 632 014, India
[2]Centre for Biomedical Engineering, S.G.N. Educational Foundation, #12, III Street, Park Avenue, Velachery, Chennai 600 042, India

The onset of tumour in biological tissues affects their optical properties. In the present study Monte Carlo simulation of the diffuse surface reflectance and transmittance for detection of the inhomogeneities/ tumour in control tissue is carried out. From the isolated heart, spleen and adipose tissues of goat digital phantoms are prepared. The virtual optical probe consists of a photon injection port (source), three ports placed along the *x*-axis at 2, 4 and 6 mm to collect backscattered photons and one port placed coaxially to the source port at the exit end to collect transmitted photons. Two types of inhomogeneities of diameter 2 mm are introduced in the phantoms – first a tissue of absorption coefficient 10% more than that of heart and same scattering coefficient; second, adipose or spleen tissue, embedded in heart phantoms, at depths 2, 4 and 6 mm. The inhomogeneity placed at depth 2 mm gives maximum normalized backscattered intensity (|NBI|) at the port placed at 2 mm. The maxima of low |NBI|s are also observed at ports located at 4 and 6 mm of inhomogeneities embedded at depths 4 and 6 mm. The signals due to high scattering and high absorption are positive and negative with reference to that of heart. The transmittance also shows respective variations with placement of tissues in the phantoms. The normalized transmitted intensity is maximum when the tissues are placed close to the exit surface. These are further characterized by the peak intensity and full-width at half maximum of signals. The data analysis provides details of their type, location and size. Inhomogeneities with minimal change in optical parameters are also identified.

Keywords: Backscattering, biological tissues, digital phantoms, transillumination, tumour.

IN the present study, Monte Carlo simulation (MCS) of the diffuse surface reflectance and transmittance to determine the extent of changes due to inhomogeneities/ tumour in control tissue is carried out. The virtual optical probe consists of a photon injection port (source), three ports placed along the *x*-axis to collect backscattered photons and one port placed coaxially to the source port at the exit end to collect transmitted photons. Adipose, highly scattering, and spleen, highly absorbing tissues are taken as inhomogeneities and heart is taken as a control tissue. Two types of inhomogeneities of diameter 2 mm are introduced in the phantoms – first, a tissue of absorption coefficient 10% more than that of heart and same scattering coefficient; second, adipose and spleen, embedded in heart phantom at depths 2, 4 and 6 mm. After injection of photons, the backscattered photons are collected by three ports placed at 2, 4 and 6 mm from the source. For 10% increase in tissue parameters all the spheres located at depth 2 mm are detected by the first port at 2 mm and are selectively detected by other ports. For adipose and spleen the absolute value of normalized backscattered intensity (|NBI|) and detection capability of deeply embedded tissues by different ports are increased. The inhomogeneity placed at depth 2 mm gives maximum (|NBI|) at the port placed at 2 mm. The maxima of lower |NBI|s are observed at other ports by placing the tissues at increased depths, 4 and 6 mm. The |NBI| increases with the increase in size of the adipose inhomogeneity and is maximum for diameter 5 mm. The normalized transmitted intensity (NTI) is maximum when the tissues of diameter 2 mm are placed close to the exit surface. These are further characterized by peak intensity and full-width at half maximum (FWHM). The analysis provides details of type, location and a parameter related to size. Inhomogeneities with minimal change in optical parameters by backscattering ports are also identified.

Laser interaction with biological tissues is a complex process. There are several mechanisms of radiation interaction with tissues such as backscattering, transmission and absorption within the medium. These interactions depend on laser wavelength, and optical properties of tissues such as refractive index, absorption and scattering coefficients and anisotropy parameter. The laser transmission is further associated with collimated and diffuse transmission[1]. Transillumination is similar to transmission but is attributed to illumination of a volume through multiple interactions near the exit end of tissues[2].

Biologically all tissues possess microstructure thus contributing to their inhomogeneous nature, but for

*For correspondence. (e-mail: msingh_iitm@yahoo.com)

macro-modelling these tissues are considered to be homogeneous with their unique optical properties as determined by experimental[3] and simulated[4,5] procedures. During the development of tumour or tissue inhomogeneity, attributed to change in local cellular growth process, the abnormal growth develops into a complex tissue with its own distinct optical properties[6]. Its detection at the onset stage by X-ray and ultrasonic technique does not produce any significant change in attenuation coefficient and acoustic impedance respectively, whereas these changes are detected by optical techniques, operating within the therapeutic window region (600–1300 nm)[7]. Based on this principle several experimental techniques have been developed to detect the tumour as it grows within the tissues[8–10].

Theoretical simulation of the process is an essential part to strengthen our understanding of tissue–photon interaction and is generally carried out by diffusion theory[11], finite element method[12] and MCS[13]. Some of the prominent results achieved by these procedures include near infrared radiation propagation in tissues, multilayer tissue scattering, influence of refractive index variation, laser–tissue interaction, detection of breast cancer, determination of optical parameters of tissues, etc. In contrast to other methods, MCS is often preferred as it provides details of photon interaction at individual level, even close to the beam entry point[2]. These photons emerge at various distances from the beam entry point and the surface profile constructed by these is a unique representation of tissue optical properties[5].

In our previous studies on MCS of laser backscattering from a simulated tissue phantom, we have shown that the radiations emerging closer to the beam entry point originates from lower depths, whereas those emerging far away are the result of interactions taking place in deeper layers in tissues[14]. Based on this we designed a laser multiprobe system which has successfully been used for various applications[15]. Some of these include imaging of tissue composition changes in various layers of human organs[16,17], development of optical tissue-equivalent phantoms[18], and localization of internal organs in the thorax region[19].

The presence of tumour in tissues, depending on their optical properties and location produces changes in back- and forward-scattering of photons. In the backscattering process these could be measured as changes in signals originating at various locations on the entry surface. Similarly, the change in transmitted signal is attributed to the presence of inhomogeneity in the tissues. But further details for effective utilization of functional capability of backscattering multiprobe and transmission techniques are required, which may help in the detection of tumour not only at the onset stage but also after it has developed in the tissues. As MCS is an established procedure for analysis of these processes, the objective of the present work is to apply this simulation for detection of inhomogeneities in tissue phantoms in terms of various parameters.

Materials and methods

Tissue phantoms

For this study adipose, spleen and heart tissues of goat were chosen. Heart tissue was used as the control, whereas adipose and spleen as inhomogeneities representing tissues with high scattering and absorption respectively. Table 1 shows these tissues with optical parameters: scattering (μ_s) coefficient, absorption (μ_a) coefficient and anisotropic parameter (g). Three types of phantoms were made. In one type, to simulate the onset of absorbing type of inhomogeneity, the absorption coefficient at a selected location of diameter 2 mm in control tissue was increased by 10% while keeping its scattering coefficient constant. Three such inhomogeneities at depths 2, 4 and 6 mm at various locations along the centre line were introduced in the phantom. For another set of phantom, the inhomogeneities of diameter 2 mm of spleen and adipose tissues below its centre at various depths were embedded, which represents fully grown abnormalities that are absorbing and scattering types. In the third phantom adipose tissue as spheres of diameter 1–5 mm was individually introduced below the centre as inhomogeneity. These control phantoms consisting of adipose and spleen tissues at various depths will hereafter be referred to as H+a and H+s respectively.

Model of scanning system

Figure 1 *a* shows the schematic of the scanning system with a phantom of homogeneous control tissue of infinite dimensions in x- and y-directions, and with a selected slab of size $30 \times 10 \times 10$ mm superposed on this. The scanning head consisted of a photon injecting port and three output ports at distances 2, 4 and 6 mm from the input port to collect backscattered photons. The input and output ports were placed in a straight line along the x-axis. To receive transmitted photons, another port was placed coaxially to the input port at the exit surface of the phantom. The photons were injected at the input port, which after interaction emerged as backscattered components collected by three ports and as transmitted component

Table 1. Optical parameters of adipose, spleen and heart tissues of goat

Organ/tissue	Scattering coefficient (cm^{-1})	Absorption coefficient (cm^{-1})	Anisotropy parameter
Heart	100.03	1.27	0.990
Spleen	109.86	4.0	0.995
Adipose	419.92	1.5	0.994

collected by a single port placed along the z-axis (Figure 1 *b*). The area of each port was 1 mm^2. One million photons of wavelength 632.8 nm were injected into the phantom through the input port. For scanning of phantoms the probe was placed at the first location and after completion of operation at this position, the scanning head was shifted to the next location 1 mm away along the x-axis. At this position also one million photons were introduced and the number of transmitted and backscattered photons at various locations was counted. This process was repeated till the scanning head reached another end of phantom (30 mm from the first position).

For detection of inhomogeneity of 10% increase in absorption coefficient, three such inhomogeneities were introduced in a straight line at depth 2, 4 and 6 mm. In a single scan starting from the initial position (x = –15 mm) to the final position (x = 15 mm), MCS for one million photons for each position was performed[20] and the photons undergoing scattering were counted. For the second study the control tissue phantom was embedded with adipose or spleen tissue of 2 mm diameter, located below the centre of the phantom (0, 0, 0) at depths 2, 4 and 6 mm. Initially adipose was embedded at location (0, 0, 2 mm), followed by its placement at (0, 0, 4 mm) and (0, 0, 6 mm). MCS was performed for each position and backscattered and transmitted photons were counted. By a similar procedure spleen tissue was embedded at locations (0, 0, 2 mm), (0, 0, 4 mm) and (0, 0, 6 mm) and simulation for the same number of photons was performed. To observe the effect of variation of size, five phantoms with spheres of adipose inhomogeneity of diameters 1, 2, 3, 4 and 5 mm respectively, were prepared. Each phantom contained only one sphere which was placed at (0, 0, 2 mm). By simulation procedure the backscattered photons from these phantoms were counted.

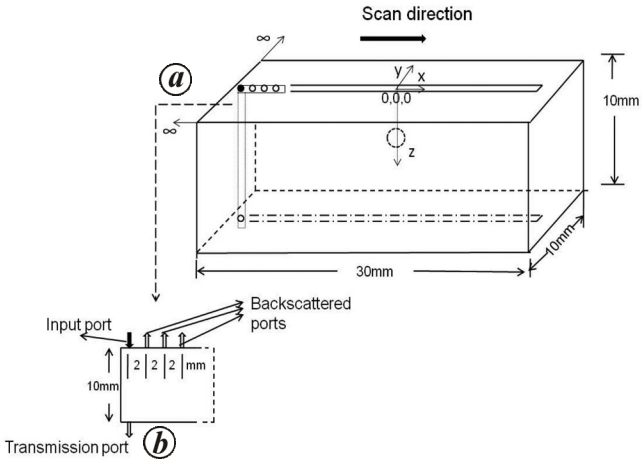

Figure 1. ***a***, Schematic of the optical scanning system for measurement of backscattered and transmitted photons after interacting with tissues. ***b***, The unit consists of five ports, one for photon injection and three to collect backscattered photons at various distances from beam entry port and one to collect transmitted photons located coaxial to the input port.

Data processing

From the number of backscattered photons collected within 1 mm^2 around the grid point (|NBI|), in terms of percentage was calculated by

$$\text{NBI}(\%) = (N_i/N_0) \times 100,$$

where N_0 is the total number of incident photons, and N_i is the total number of photons collected at position i.

The |NBI| values as obtained at various grid points, along with their positions were stored in the computer for further processing[5]. Similarly, the number of transmitted photons collected within 1 mm^2 grid point at the corresponding position i was counted and represented as NTI

$$\text{NTI}(\%) = (T_i/N_0) \times 100,$$

where N_0 is the total number of incident photons, and T_i is the total number of photons collected at position i by the transmission port. The NTI values were stored in the computer along with their positions for further processing.

Monte Carlo simulation

Figure 2 shows the flow chart of MCS. This is a stochastic procedure that can be applied to any random event in nature. Here it has been used to simulate the light transport by injecting photons or photon packets on a random walk through biological tissues. The photon was treated as a neutral particle and its movement was governed by the mean free path, scattering and absorption coefficients, and anisotropy parameter[20]. The photons after multiple interactions emerged as backscattered and transmitted

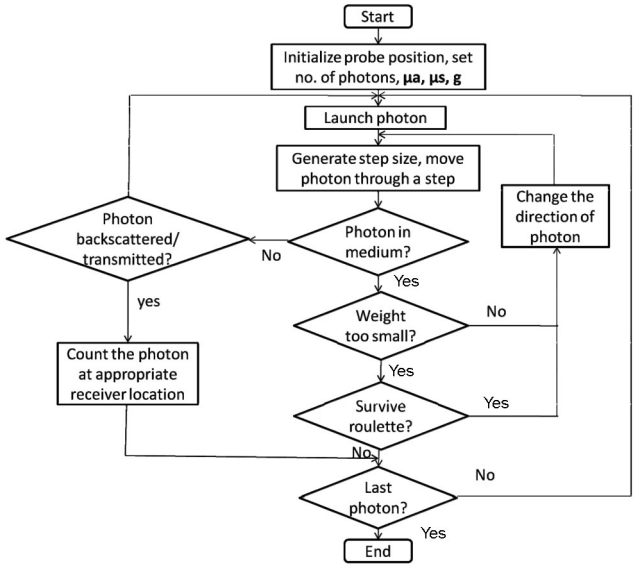

Figure 2. Flow chart of Monte Carlo simulation.

components on the top and exit surfaces respectively. The code for MCS was written in C^{++}. Total time taken for a complete operation of one million photons was approximately 2 h and 15 min.

The photons were introduced perpendicular to the surface for maximizing their entry and minimizing the surface reflection, undergoing diffuse backscattering and transillumination process (Figure 3). Each photon, out of one million, was initialized with a weight of unity, which corresponds to the collimated ray of incident photons. The step-size s of the photon was calculated using a generated random variable ς given by

$$s = (-\ln \varsigma/\mu_t) \text{ and } \mu_t = \mu_a + \mu_s, \quad (1)$$

where μ_t, μ_a, μ_s are the total attenuation, absorption and scattering coefficients of the medium respectively. The value of the random number ς was between 0 and 1. The deflection angle θ was calculated as

$$\cos\theta = \frac{1}{2g}\left[1 + g^2 - \left\{\frac{(1-g^2)}{(1-g+2g\varsigma)}\right\}^2\right] \quad \text{for } g \neq 0, \quad (2)$$

$$\cos\theta = 2\varsigma - 1 \quad \text{for } g = 0, \quad (3)$$

where g is the anisotropy parameter of the medium. The azimuthal angle ψ is given by

$$\psi = 2\pi\gamma, \quad (4)$$

where γ is a random variable between 0 and 1.

The path length of the first interaction of the photon was found, and thereafter it was moved. If the photon had left the tissue, the possibility of its presence at one of the receiving ports was checked. If detected, a counter was incremented to count the photon received by the corresponding port. If the photon was internally reflected, then the photon location was updated and the program continued. With each step the photon weight was reduced due to absorption by the tissue. The amount of weight lost, ΔQ, in absorption was given by

$$\Delta Q = W(\mu_a/\mu_t), \quad (5)$$

where W is the total weight of the photon. The photon weight and direction after scattering were updated. The new position of the photon (x', y', z') from the previous position (x, y, z) was given by

$$\begin{pmatrix} x' \\ y' \\ z' \end{pmatrix} = \begin{pmatrix} x \\ y \\ z \end{pmatrix} + s\begin{pmatrix} \sin\theta\cos\psi \\ \sin\theta\sin\psi \\ \cos\theta \end{pmatrix}. \quad (6)$$

If the photon weight falls below a minimum threshold ($W_c = 0.001$), it was subjected to roulette condition for elimination. Further details of this simulation are given elsewhere[20].

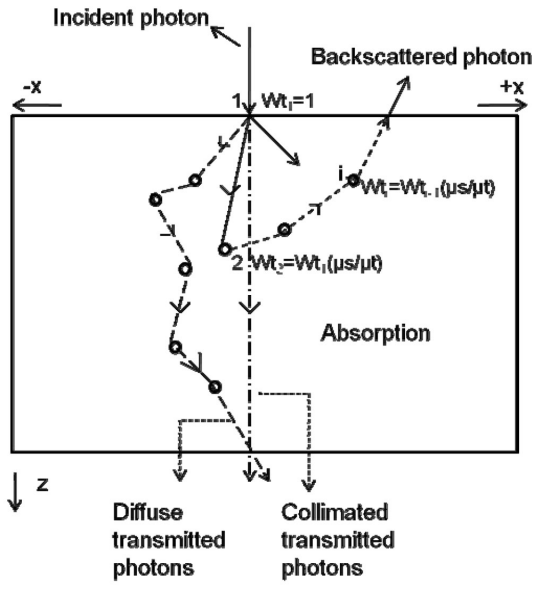

Figure 3. Model of photon propagation through the tissue medium.

Data acquisition and processing

The optical probe was implemented by performing the MCS of light photon propagation in tissues. Initially at position $x = -15$ mm, 1 million photons by input port were injected into the tissue phantom. The photons that reach the backscattering and transmitted output ports were counted and converted into |NBI| and NTI respectively. Thereafter, the probe was moved by 1 mm along the x-axis to the next location and the photons were injected through the input port. At each source location MCS for photon transport was performed. In this manner the entire length of tissue phantom up to $x = 15$ mm was scanned. The photons detected by the ports were stored in four files, one for the transmission port and three for the backscattering ports.

For determination of the changes in |NBI| due to placement of adipose spheres of various sizes below the origin, MCS by the above procedure was carried out. After completion of data acquisition with sphere of 1 mm, the same procedure was repeated with spheres of diameter ranging from 2 to 5 mm.

Prior to signal analysis, the |NBI| and NTI data were collected from control phantom at three backscattering and one transmission ports. These data were subtracted from the data collected from the phantoms with inhomogeneities placed at various depths. By this procedure the associated noise with signals was minimized[21]. Finally the |NBI| and NTI signals with position on the phantoms were plotted.

Results

Figure 4 shows |NBI| signal variation due to placement of the inhomogeneities of 10% increase in absorption coefficient, embedded at various locations in heart phantom. The |NBI| variation as received by the first, second and third ports is shown in Figure 4 *a–c* respectively. At the port located at 2 mm, the first signal with high |NBI| is received. This is followed by the signals as detected by the port at 4 mm. All three inhomogeneities are detected, but |NBI| is corresponding to the inhomogeneity located at 4 mm is higher compared to that at other depths. At 6 mm port the signal corresponding to inhomogeneity placed at 6 mm is only observed.

Figure 5 shows |NBI| variation for different phantoms with inhomogeneities placed at various locations. |NBI| obtained with adipose placed at 2 mm is the maximum. With placement of inhomogeneity at depth 4 mm, |NBI| is reduced. With increase in depth of placement to 6 mm, |NBI| is further reduced. The scans of phantoms with spleen embedded at various depths show negative values of |NBI| compared to those of adipose tissues, attributed to its high absorption. The maximum |NBI| in each plot occurs away from the origin. This is attributed to the position of the first collection port, which is 2 mm away from the injection port.

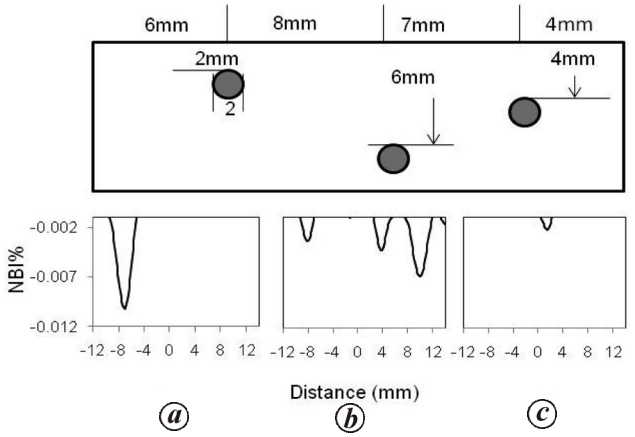

Figure 4. Placement of the inhomogeneities with 10% increase in absorption coefficient of heart while retaining the scattering coefficient constant, embedded at various locations. ***a–c***, The |NBI| variation as received at the first, second and third ports respectively. At 2 mm the first, at 4 mm all three but with increased |NBI| corresponding to 4 mm position and at 6 mm port the inhomogeneity placed at 6 mm only are observed.

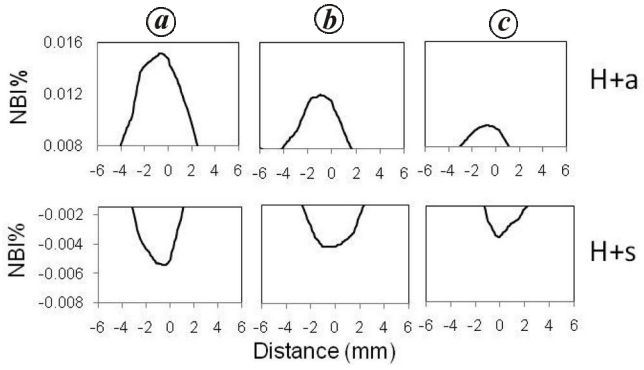

Figure 5. The scans of |NBI| along the *x*-axis of phantoms with inhomogeneities placed at (***a***) (0, 0, 2 mm), (***b***) (0, 0, 4 mm) and (***c***) (0, 0, 6 mm) measured at ports placed at 2, 4 and 6 mm away from the injection port respectively.

Considering the homogeneous nature of the heart and adipose tissues, their 3D plots were constructed. The occurrence of maximum |NBI| for adipose, along with its distribution at various locations, is shown in Figure 6. Due to high scattering within the tissues, |NBI| shows reduction at ports located at 4 and 6 mm. Similar plots are also made for spleen spheres placed at various depths in control phantoms.

The |NBI| peak intensities (PI_B) and full-width at half maximum due to backscattered photons ($FWHM_B$) were compared for the phantoms with inhomogeneities placed at various depths (Table 2). $FWHM_B$ was calculated from |NBI| variation with respect to scanning distance. PI_B was high for adipose compared to that of spleen, placed at various depths, attributed to its high scattering. $FWHM_B$ was maximum for adipose placed at 2 mm, whereas it was minimum for spleen embedded at depth 6 mm. These parameters are related to size of the inhomogeneity, but are affected by optical scattering.

Figure 7 shows NTI variation for inhomogeneities embedded in control tissue phantom at various depths. The change in NTI is attributed to the type of tissue embedded in this. Due to high forward scattering distinct peaks from the adipose tissue phantom are observed. On the other hand, for spleen high absorption leads to broadening of signal with lesser NTI values. The NTI signal emerging after placement of inhomogeneities at 6 mm is lower for spleen compared to that of adipose tissues. Figure 8 shows the 3D variation of inverted NTI. The minimum NTI values are observed at the centre. Due to homogeneous nature of various tissues, a symmetric shape of these plots is observed, highlighting the distribution of NTI at various locations.

Based on NTI signals from various tissue phantoms, PI_T and $FWHM_T$ were calculated (Table 3). PI_T is minimum when the inhomogeneities are embedded at 6 mm and maximum for 2 mm, which is primarily attributed to the multiple scattering within the medium. PI_T with increasing depth of placement of tissues in the phantoms is less for adipose at 2 and 4 mm, and more at 6 mm compared to that of spleen. $FWHM_T$ shows a decreasing trend with increasing depth of placement of inhomogeneities in tissues, but this change is more for spleen compared to that for adipose.

For determination of the effect of variation in the size of inhomogeneity on the above parameters, several simulation studies of the backscattering process were carried out. From the |NBI| plots, PI and FWHM were calculated.

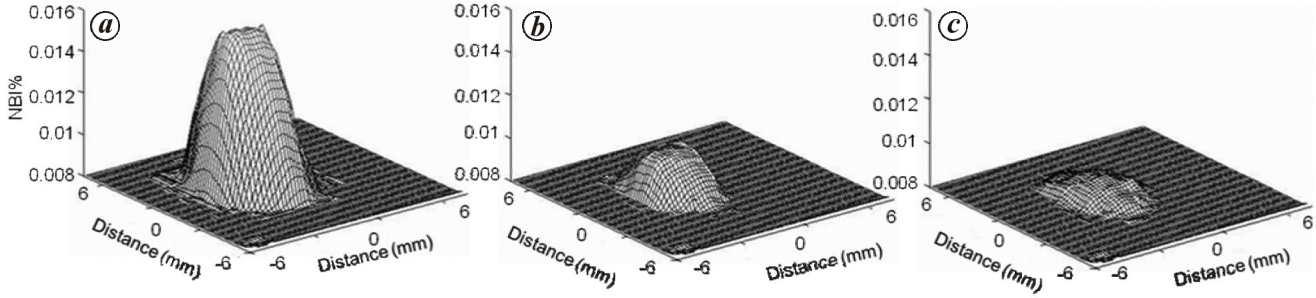

Figure 6. 3D plots of |NB| along the *x*-axis of H+a phantoms with inhomogeneities placed at (***a***) (0, 0, 2 mm), (***b***) (0, 0, 4 mm) and (***c***) (0, 0, 6 mm) measured at ports placed at 2, 4 and 6 mm away from the injection port respectively.

Table 2. Peak intensity (PI_B) and full-width at half maximum ($FWHM_B$) of the data collected by the backscattered ports when adipose and spleen tissues of diameter 2 mm are embedded inside the control tissue at various depths

	PI_B		$FWHM_B$ (mm)	
Depth (mm)	Adipose	Spleen	Adipose	Spleen
(0, 0, 2)	0.015	0.0056	5.375	3.25
(0, 0, 4)	0.009	0.0043	3.35	2.875
(0, 0, 6)	0.0044	0.00367	2.85	1.75

Table 3. Peak intensity and FWHM from the data received at the transmission port from phantoms with adipose and spleen of diameter 2 mm

	PI_T		$FWHM_T$ (mm)	
Depth (mm)	Adipose	Spleen	Adipose	Spleen
2	0.928	0.6396	4.9	6.25
4	1.367	0.9559	3.875	5.625
6	1.587	1.837	3.75	4.625

Table 4. Variation of PI_B and $FWHM_B$ for adipose inhomogeneity of different diameters placed at 2 mm depth, as determined from the NBI scans

Diameter of adipose tissue (mm)	PI_B	$FWHM_B$ (mm)
1	0.0061	2.500
2	0.0152	4.875
3	0.0293	4.500
4	0.0538	5.000
5	0.0724	5.625

Table 4 shows the effect of change in size of the adipose inhomogeneity placed in the control phantom at a depth of 2 mm on PI_B and $FWHM_B$. The initial increase in $FWHM_B$ is followed by a decrease with increase in the size of the inhomogeneity. In contrast, a smooth increase is observed in PI_B for adipose tissues.

Discussion

The laser radiation–tissue interaction is associated with several parameters such as layered tissue structure,

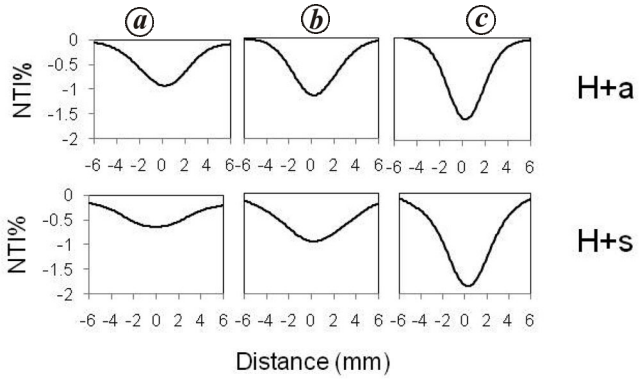

Figure 7. The scans along the *x*-axis of H+a and H+s phantoms with inhomogeneities placed at (***a***) (0, 0, 2 mm), (***b***) (0, 0, 4 mm) and (***c***) (0, 0, 6 mm).

refractive index variation within the layers, optical parameters of each layer and wavelength of light source. MCS offers a flexible approach to photon transport in turbid tissues, which describes local rules of photon propagation that are expressed as probability distributions. As this method is statistical in nature, it relies on calculating the propagation of a large number of photons using the computer, which requires a large amount of computational time[13].

The scattering of electromagnetic radiation increases with increase in wavelength within the therapeutic window region[22]. This further depends on the optical parameters of the biological tissues. The present study shows that the basic interaction mechanism is not changed even at 10% increase in absorption coefficient and its presence is still being detected. This means that detection capability of optical scattering is sensitive to tissue compositional changes. This also shows that the multiport system is still capable of identifying objects placed at different depths. With increase in depth the scattering increases, leading to reduced |NBI| signal.

The present study is based on optical backscattering and transillumination from the phantoms embedded with inhomogeneities. The backscattering forms a fraction of the transmitted component. Initially the backscattering (a time-dependent process) is confined to closer regions, but

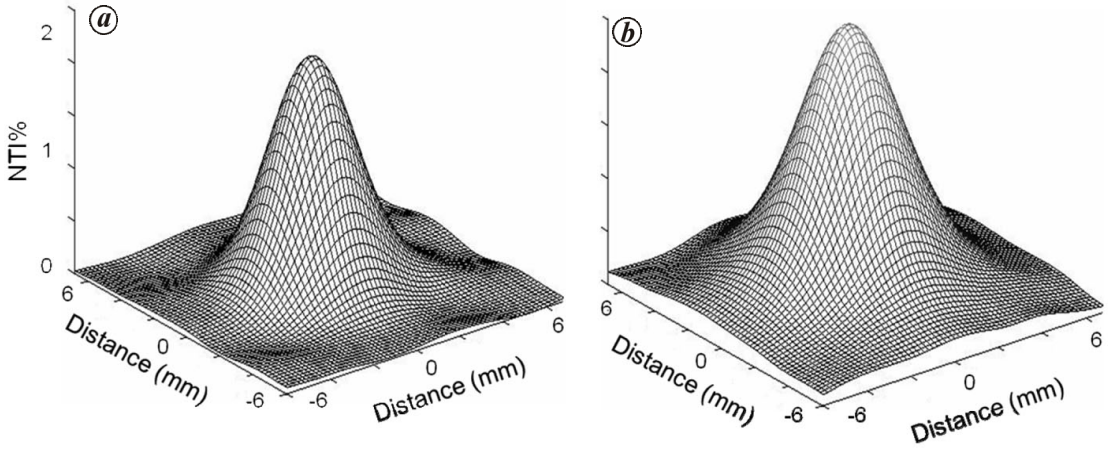

Figure 8. 3D plots of phantoms (***a***) H+a and (***b***) H+s with inhomogeneities placed at (0, 0, 6 mm).

with increase in time duration the number of scattered photons at farther distances from the input port also increases[23]. This is attributed to multiple interactions and absorption within the tissues. Based on the number of photons reaching different ports a surface profile is formed, which is used to determine optical parameters of the tissues[24]. Due to embedding of inhomogeneities in tissues, the surface profiles of the corresponding region are changed. Further change occurs due to shift in their positions in the phantoms, leading to shift in the occurrence of maximum, primarily attributed to their optical properties and absorption of photons within the tissues. All tissues exhibit the respective maximum |NBI| at various ports depending on the placement of inhomogeneities but for H+a phantom this is positive compared to H+s phantom. Thus by this procedure the effects of inhomogeneities are identified. Similar analysis has been effectively used in determining the tissue changes in epithelium below the surface[25].

Through the movement of probe and placement of inhomogeneity the respective |NBI|s are obtained. 3D plots of these are not symmetric, which is attributed to the statistical fluctuations in the collection of photons and location of the ports with respect to photon injection port. The maximum |NBI| occurs when the photon injection port is located at the origin (above the inhomogeneity), and collection ports are located off-centre. $FWHM_B$, is affected by the scattering, which decreases with the depth of placement of inhomogeneity. For spleen these values are less and negative compared to that of adipose, showing the effect of high absorption.

$FWHM_B$ and PI_B increase with the size of the adipose inhomogeneity placed at a fixed depth. This is attributed to the increase in backscattering due to increase in size, thus leading to higher values of these parameters. The percentage change in PI_B increases with the change in size from 1 to 5 mm, but due to its complex variation no proportionality factor related to size could be established.

In transmission mode, due to prominence of forward scattering, higher NTIs are observed for H+a and H+s phantoms at all depths of placement of inhomogeneity compared to that of |NBI| values. After placing this at 6 mm, NTI is less for H+s than for H+a phantom, which is attributed to enhanced scattering of adipose inhomogeneity. This is despite the high refractive index of adipose tissues. For H+s phantom the refractive index of heart is the same as that of spleen, thus allowing the photons to follow their paths without deviation. This process is further associated with high absorption of multiple scattered photons within the spleen and transmitting others through the heart tissue, leading to low PI_T and $FWHM_T$ compared to that of adipose tissue. The transillumination at the exit surface is symmetrical around the *z*-axis, irrespective of the type of inhomogeneity embedded in the phantom, as shown by their 3D plots. The increased/decreased scattering affects the transillumination to a varying degree which is related to the object size[26]. Due to complexities of the scattering process no proportionality of $FWHM_T$ with size could be established with increasing depth of embedding of inhomogeneity. The blurring caused by multiple scattering is one of the prominent factors affecting the size determination of the objects[27].

In conclusion, the present study shows that the basic mechanism of radiation interaction with inhomogeneities remains the same. When the change is less in optical parameters, |NBI| is proportionally altered. The placement at different depths in tissue leads to a distinct pattern of backscattered signal, as measured by multiport system, indicating their type and position in the phantom. The signal is associated with less noise if the inhomogeneity is located close to the beam entry surface. On the other hand, the transmitted signal is associated with less noise if the inhomogeneity is located close to the exit surface of tissues. In contrast to optical coherence tomography[28], this procedure may help in detecting tumour in various layers of soft tissues. Further analysis of the

signals may provide details regarding optical properties[29] and the role of inhomogeneous nature of the tissues[30].

1. Tuchin, V. V., Light scattering study of tissues. *Physics-Uspekhi*, 1997, **40**, 495–515.
2. Patwardhan, S. V., Dhawan, A. P. and Relue, P. A., Monte Carlo simulation of light-tissue interaction: three-dimensional simulation for transillumination-based imaging of skin lesions. *IEEE Trans. Biomed. Eng*., 2005, **52**, 1227–1236.
3. Pickering, J. W., Prahl, S. P., Van Wieringen, N., Beck, J. F., Storenborg, H. J. C. M. and van Gemert, M. J. C., Double integration sphere system for monitoring of optical properties of tissues. *Appl. Opt.*, 1993, **32**, 399–410.
4. Cui, W. and Ostrander, L. E., The relationship of surface reflectance measurements to optical properties of layered biological media. *IEEE Trans. Biomed. Eng.*, 1992, **39**, 194–201.
5. Kumar, D. and Singh, M., Characterization and imaging of compositional variation in tissues. *IEEE Trans. Biomed. Eng.*, 2003, **50**, 1012–1019.
6. Charvet, I. *et al.*, A new optical method for the noninvasive detection of minimal tissue alterations. *Phys. Med. Biol*., 2002, **47**, 2095–2108.
7. Srinivasan, R. and Singh, M., Laser backscattering and transillumination imaging of human tissues and their equivalent phantoms. *IEEE Trans. Biomed. Eng*., 2003, **50**, 724–730.
8. Gibson, A. P., Hebden, J. C. and Arridge, S. R., Recent advances in diffuse optical imaging. *Phys. Med. Biol.*, 2005, **50**, R1–R43.
9. Guo, Z., Wan, G. S. K. W., August, D., Ying, A. J., Dunn, S. M. and Semmlow, J. L., Optical imaging of breast tumor through temporal log-slope difference mapping. *Comput. Biol. Med*., 2006, **36**, 209–223.
10. Srinivasan, R., Kumar, D. and Singh, M., Optical characterization and imaging of biological tissues. *Curr. Sci.*, 2004, **87**, 218–227.
11. Fantini, S., Walker, S. A., Franceschini, M. A., Kaschke, M., Schlag, P. M. and Moesta, K. T., Assessment of the size, position, and optical properties of breast tumors *in vivo* by noninvasive optical methods. *Appl. Opt*., 1998, **37**, 1982–1989.
12. Aridge, S. R., Schweiger, M., Hiraoka, M. and Delpy, D. T., A finite element approach for modeling photon transport in tissue. *Med. Phys.*, 1993, **20**, 299–309.
13. Wang, L., Jacques, S. L. and Zheng, L., MCML – Monte Carlo modeling of light transport in multi-layered tissues. *Comput. Methods Prog. Biomed*., 1995, **47**, 131–146.
14. Kumar, D., Chacko, S. and Singh, M., Monte Carlo simulation of photon scattering in tissue models. *Indian J. Biochem. Biophys.*, 1999, **36**, 330–336.
15. Chacko, S. and Singh, M., Multi-layer imaging of human organs by measurement of laser backscattered radiations. *Med. Biol. Eng. Comput.*, 1999, **37**, 278–284.
16. Nandakumar, S. and Singh, M., Non-invasive imaging and characterization of human foot by multi-probe laser reflectometry and Monte Carlo simulation. *Med. Biol. Eng. Comput.*, 2005, **43**, 313–318.
17. Pandian, P. S., Kumaravel, M. and Singh, M., Optical imaging and parametric characterization of frostbite changes in human hand tissues. *Curr. Sci*., 2008, **95**, 196–203.
18. Anand, N. S., Kumar, D., Srinivasan, R. and Singh, M., Laser reflectance imaging of human forearms and their tissue-equivalent phantoms. *Med. Biol. Eng. Comput*., 2003, **41**, 28–32.
19. Pandian, P. S., Kumaravel, M. and Singh, M., Laser reflectance imaging of human chest for localization of internal organs. *IEEE Trans. Biomed. Eng*., 2010, **57**, 1167–1175.
20. Jacques, S. L. and Wang, L., Monte Carlo monitoring of light transport in tissues. In *Optical Thermal Response of Laser-Irradiated Tissue* (eds Welch, A. J. and van Gemert, M. J. C.), Plenum Press, New York, 1995, pp. 73–103.
21. Gonzalez, R. C. and Woods, R. E., *Digital Image Processing*, Addison-Wesley, MA, USA, 1993, pp. 331–390.
22. Cheong, W. E., Prahl, S. A. and Welch, A. J., A review of the optical properties of biological tissues. *IEEE J. Quant. Electron*, 1990, **26**, 2166–2184.
23. Tromberg, B. J. *et al.*, Non-invasive in vivo characterization of breast tumors using photon migration spectroscopy. *Neoplasia*, 2000, **2**, 26–40.
24. Pandian, P. S. and Singh, M., Localization and characterization of tissue changes by laser backscattering and Monte Carlo simulation. *Indian J. Exp. Biol*., 2010, **48**, 993–1001.
25. Cohen, F. S., Taslidere, E. and Murthy, S., Can we see epithelium tissue structure below the surface using an optical probe? *Med. Biol. Eng. Comput*., 2011, **49**, 85–96.
26. Michielsen, K., De Raedt, H. and García, N., Computer simulation of time-gated transillumination and reflection of biological tissues and tissue-like phantoms. *Med. Phys*., 1997, **24**, 1688–1695.
27. Moscoso, M., Keller, J. B. and Papanicolaou, G., Depolarization and blurring of optical images by biological tissue. *J. Opt. Soc. Am. A*, 2001, **18**, 948–960.
28. Gonzalez-Rodrıguez, P. and Kim, A. D., Reflectance optical tomography in epithelial tissues. *Inverse Problems*, 2009, **25**, 015001-24.
29. Pfefer, T. J., Bennett, S. L. M., Gall, C. L., Wilke, J. A., Durkin, A. J. and Ediger, M. N., Reflectance-based determination of optical properties in highly attenuating tissue. *J. Biomed. Opt*., 2003, **8**, 206–215.
30. Trivedi, A., Basu, S. and Mitra, K., Temporal analysis of reflected optical signals for short pulse laser interaction with nonhomogeneous tissue phantoms. *J. Quant. Spectr. Radiat. Transfer*, 2005, **93**, 337–348.

Received 7 March 2014; revised accepted 23 August 2014